Adsorption of Methylene Blue Dye Using Biochar Derived from Finger Millet Waste Biomass: Kinetics, Isotherms, and Thermodynamic Studies

Kalaivani Kaliannan[1*], Saravanan Kaliannan[2]

[1]Department of Chemical Engineering, Kongu Engineering College, Perundurai, Erode, Tamilnadu, India

[2]Department of Pharmaceutical Technology, Shree Venkateshwara Hi-Tech Engineering College, Gobichettipalayam, Erode, Tamilnadu, India

Corresponding author: e-mail: kalaijegu@gmail.com

Graphical abstract

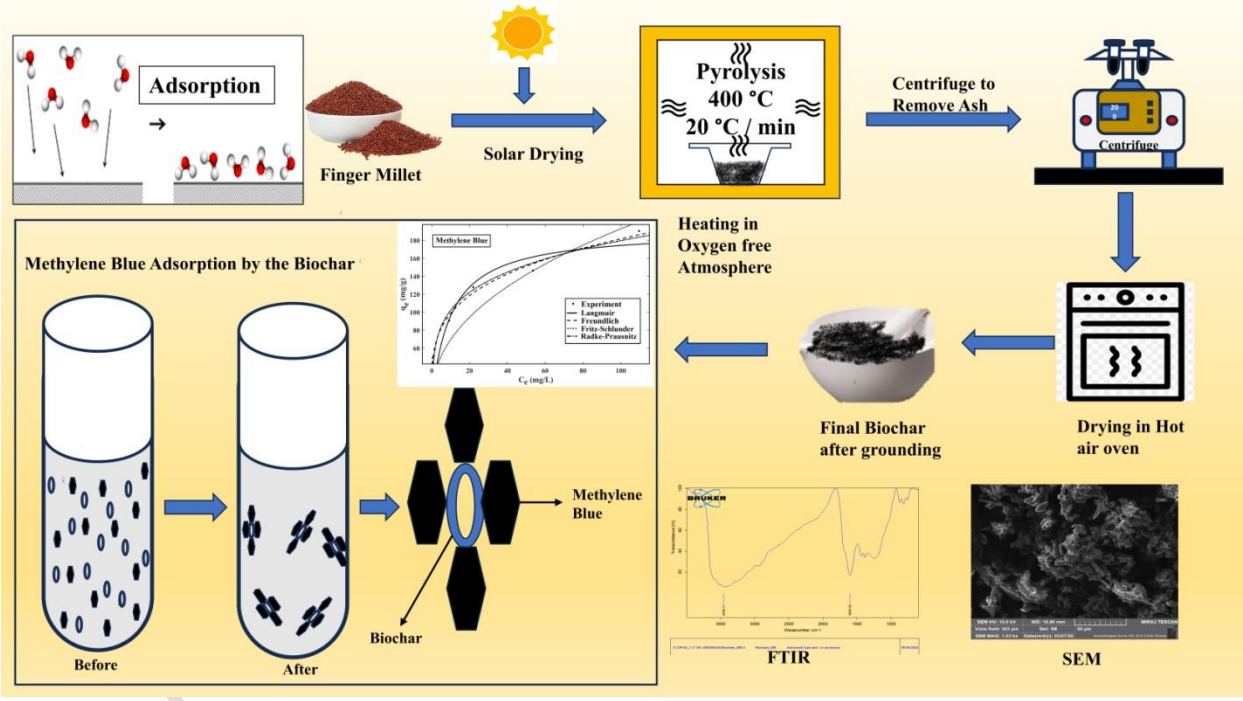

Abstract:

Globally, synthetic dyes contribute to significant environmental contamination due to their toxicity, durability, and resistance to conventional treatment processes. Therefore, there is a need to adopt best practices for remediation. Our study examines the potential of biochar produced from Finger Millet Waste Biomass (FMWB) as an effective and environmentally sustainable adsorbent material for the uptake of Methylene Blue (MB) from aqueous solutions. The characterisation of the biochar's physicochemical properties- specifically, surface morphology, porosity, and functional groups- is conducted using Fourier Transform Infrared Spectroscopy (FTIR), X-ray Diffraction (XRD), Scanning Electron Microscopy coupled with Energy Dispersive X-ray Spectroscopy (SEM-EDX), Particle Size Analysis (PSA), and zeta potential. The adsorption processes are systematically optimised, taking into account various factors such as pH, sorbent dose, initial dye concentration, contact time, and temperature. The adsorption efficiency for MB correlates with the initial increase of biochar dose, reaching a saturation plateau at 1 g/L, with 100% removal observed at an optimal pH of 7–8, and the adsorbent exhibited a maximum adsorption capacity of 191.8 mg/g confirming its potential as a sustainable adsorbent for dye-laden wastewater. As the feed dye concentration increases, adsorption efficiency decreases, suggesting monolayer adsorption dominates at lower concentrations. Isotherm analysis suggests that the Freundlich model best described the process (with R^2=0.9877), indicating heterogeneous multilayer adsorption. Kinetic modeling confirms chemisorption, with a pseudosecond-order mechanism being predominant. Thermodynamic analysis reveals the exothermic and spontaneous nature of the adsorption process. The findings ~~of this study~~ indicate that biochar derived from finger millet possesses a substantial potential for application as an adsorbent in wastewater treatment processes. This is attributed to its notable adsorption efficiency, economic viability, and sustainability attributes.

Keywords: Adsorption, Biochar, Finger Millet, Freundlich isotherm, adsorption efficiency.

Introduction:

The textile dyeing industry is a major contributor to water pollution, primarily through the discharge of untreated effluents rich in stable and toxic synthetic dyes, notably azo dyes, which pose significant risks to both human health and aquatic ecosystems (Raman & Kanmani, 2018; Macchi et al., 2021). These effluents not only introduce persistent organic pollutants, salts, and

acids into water bodies, but also deplete dissolved oxygen, thereby disrupting aquatic biodiversity (Nasrin et al., 2022; Islam & Mostafa, 2019; Yaseen & Scholz, 2018). While conventional wastewater treatments often fall short in removing such contaminants, bioremediation—particularly using microbes—has shown promise for dye degradation (Sarkar et al., 2017). However, adsorption remains one of the most efficient, practical, and scalable solutions for dye removal due to its operational simplicity and effectiveness across a variety of industrial contexts (Akhtar et al., 2024; Salahshoori et al., 2024). Hybrid treatment systems integrating UV irradiation, bioremediation, and adsorption have demonstrated complete contaminant removal from wastewater, reinforcing adsorption's role as a core technology in advanced water purification (Sayed et al., 2024). Like pharmaceutical compounds, Methylene Blue is an emerging pollutant whose rejection in nanofiltration is governed mainly by size exclusion and membrane properties, though natural organic matter can reduce flux and overall performance (Mohd Hanafiah et al., 2024). From an industrial perspective, textile, leather, and paper industries discharge large quantities of dye-containing effluents that pose severe environmental and health hazards. Conventional treatment methods such as coagulation–flocculation, advanced oxidation, and membrane filtration often suffer from high operational costs, incomplete removal efficiency, or secondary waste generation. In this context, adsorption is widely recognized as an efficient, scalable, and easy-to-operate alternative.

Recent advances have highlighted biochar, especially that produced from agricultural residues, as a potent adsorbent for environmental remediation (Kumar et al., 2023). In particular, biochar derived from finger millet (*Eleusine coracana*) waste biomass offers unique advantages, such as high ash content rich in silica, calcium, and potassium, a favorable surface chemistry, and a hierarchical porous structure, all of which enhance its capacity for cationic dye adsorption (Batagarawa & Ajibola, 2019). This study aims to evaluate the adsorption performance and underlying mechanisms of finger millet biochar waste which is a first of its kind for Methylene Blue removal, incorporating a comprehensive kinetic, isotherm, and thermodynamic analysis to elucidate adsorption performance and mechanisms, thereby positioning it as a sustainable solution for both pollutant remediation and agricultural value addition. ~~This study focused on the adsorption of Methylene Blue (MB) from solutions using biochar derived from finger millet, highlighting an economic and eco-friendly approach to wastewater treatment.~~ The biochar is characterized using chemical techniques such as FTIR, XRD, PSA, SEM, and surface charge

assessment via Zeta potential analysis. To evaluate the significance of the parameters affecting dye adsorption- including pH, adsorbent dose, initial dye concentration, contact time, and temperature- optimizing the batch adsorption technique proved beneficial. Sorption isotherms and kinetics modeling were conducted, and thermodynamic analysis is performed and discussed to enhance understanding of the mechanisms and effectiveness of dye removal by finger millet biochar, thereby confirming it as a suitable and cost-effective adsorbent for water treatment applications.

Materials and Methods:

Biochar Preparation from Finger Millet

The raw biomass precursor, Finger millet *(Eleusine coracana)* collected was thoroughly washed using deionised water to remove impurities and dried in the sun to eliminate excess moisture. The dried samples were placed in covered porcelain crucibles and subjected to oxygen-limited pyrolysis in a muffle furnace. The furnace maintained an approximate temperature of 400 °C with a heating rate of 20 °C/min. After pyrolysis, the resulting biochar was centrifuged 2000 rpm for 10 minutes to eliminate residual ash. The biochar was then dried in a hot-air oven at 100°C for 12 hours to obliterate any remaining moisture. The dried biochar was ground into a very fine powder using a mortar and pestle. The ~~small quantity of~~ powdered biochar was stored in an airtight container to protect it from contaminants and preserve its properties for further analysis. The biochar yield (Y_P) from the raw biomass was calculated using the following equation 1:

$$Y_P\ (\%) = (m_B / m_R) \times 100 \quad (1)$$

Where: m_B is the mass of biochar obtained after pyrolysis (g) and m_R is the initial mass of raw finger millet biomass (g).

FTIR Characterization

The properties of the prepared adsorbents were systematically investigated through the application of various analytical techniques to assess their efficiency and structural characteristics both before and after the adsorption process. Fourier Transform Infrared Spectroscopy (FTIR) (Model: 8400S, Shimadzu, Japan) was utilised to analyse the infrared spectra, with particular emphasis on the identification of functional groups and structural

modifications. During this analysis, the adsorbent was converted into Potassium Bromide (KBr) pellets and scanned over the range of 4000 to 400 cm^{-1}, employing a resolution of 4 cm^{-1}, with a pure KBr pellet functioning as the baseline.

XRD Characterization

X-ray diffraction (XRD) was employed to examine the crystalline characteristics and atomic arrangements. The patterns were acquired utilising a D8 Advance ECO XRD system, which is equipped with an SSD160 1D detector (Bruker), thereby enabling the identification of phases within the adsorbent as well as its alterations following adsorption. A reference sample designated as RFB-400 was utilised as a control.

SEM - EDX

The methodology utilized Scanning Electron Microscopy (SEM) in conjunction with Energy Dispersive X-ray Spectroscopy (EDX), specifically employing the Sigma HV model from Carl Zeiss and the Bruker Quantax 200 detector (plate number: Z10 EDS). This analytical approach aimed to comprehensively assess the surface morphology, elemental composition, and spatial distribution of elements on and proximate to the adsorbent surface. SEM facilitated high-resolution imaging of surface textures and structural modifications resultant from adsorption processes, whereas EDX allowed for the precise detection and quantification of the elemental constituents present within the biochar material. These advanced techniques collectively elucidated the topographical and compositional transformations that occur during adsorption.

Preparation of Dyes:

The pH of the dye solutions was controlled to a target value of 9.0 for Methylene Blue by adding 0.5 M sodium hydroxide (NaOH) and 0.5 M hydrochloric acid (HCl) in order to raise the pH or reduce the pH respectively. Subsequently, a precise amount of 100 mg of biochar was introduced into 50 mL of each dye solution. The resulting mixture was then transferred to a sealed flask and agitated on a rotary shaker at a speed of 150 revolutions per minute (rpm) for duration of 90 minutes to facilitate optimal adsorption. Following this period, the solution was subjected to filtration to isolate the adsorbent, and the concentration of dye in the filtrate was determined using a UV-Vis spectrophotometer at its characteristic absorption wavelength (λ_{max}) of 664 nm

(Martis et al., 2022). The final measurement indicated that the dye concentration of Methylene Blue was 0.142 mg/L.

Effect of pH

To study pH effects, 50 mL solutions of Methylene Blue (MB) at 100 mg/L were prepared. pH was adjusted to 2, 4, 6, 8, and 10 using 0.1 M NaOH or HCl. Biochar (100 mg) was added, and mixtures were agitated at 150 rpm for 60 min at room temperature. After filtration, residual dye concentrations were measured with a UV-Vis spectrophotometer. The percentage of dye removal at each pH was calculated.

Effect of Temperature

To assess temperature impact, 50 mL of MB dye solutions (100 mg/L) at optimal pH were prepared. Each received 100 mg of biochar and was agitated at 150 rpm. Experiments occurred at 300, 310, 320, and 330 K using a controlled bath or shaker. After 60 min, solutions were filtered, and residual dye concentrations analysed via UV-Vis spectrophotometer, calculating the percentage removal at each temperature.

Effect of Adsorbent Dosage

To study biochar dosage effects, 50 mL of MB dye solution (100 mg/L, optimal pH) was prepared. Adsorbent dosages of 0.1 g, 0.5 g, 1.0 g, 1.5 g, and 2.0 g were added to separate solutions. The mixtures were agitated at 150 rpm for 60 min at room temperature. After adsorption, solutions were filtered, and dye concentrations were measured with a UV-Vis spectrophotometer. The percentage of removal for each dosage was calculated.

Effect of Dye Concentration

To investigate the effect of the initial dye concentration, 50 mL dye solutions with varying concentrations (e.g., 50, 100, 150, 200, 250, and 300 mg/L) were prepared at a fixed pH and temperature. Biochar (100 mg) was added to each solution, and the mixtures were stirred at 150 rpm for 60 minutes. After adsorption, the solutions were filtered, and the residual dye

concentrations were analysed using a UV-Vis spectrophotometer. The percentage removal at different concentrations was calculated.

Effect of Contact Time

To determine the effect of contact time, 50 mL solutions of MB at a fixed concentration (e.g., 100 mg/L), pH, and temperature were prepared. Biochar (100 mg) was then added to each solution. Samples were withdrawn at specific time intervals (10, 20, 30, 40, 50, 60, and 90 min), while the solutions were continuously agitated at 150 rpm. The samples were filtered, and the dye concentrations were measured using a UV-Vis spectrophotometer. The percentage of removal at each time interval was then calculated.

Adsorption studies:

The pH of MB dye solutions was adjusted to 9 using 0.1 M NaOH or HCl. MB solution was added to the flask with 100 mg of biochar (adsorbent), which was shaken at 150 rpm for 90 minutes in a rotary shaker. Adsorbent solution concentration was measured after a specified period of filtration of the adsorbent solution. Using a UV-Vis spectrometer, optical density was measured for the filtrate, and adsorption efficiency was calculated. A variety of experimental factors were considered, including pH, initial metal ion concentration, contact time, and working temperature. The percentage of dye removed was calculated using equation 2 as given below:

$$\%Removal = \frac{C_i - C_o}{C_i} X\ 100 \quad (2)$$

C_i is the initial, and C_0 (mg L^{-1}) is the solution's final metal concentration. At any time, t, metal adsorption capacity q_t (mg/g) is calculated from equation 3.

$$q_t = (C_i - C_t) \times \frac{V}{M} \quad (3)$$

V (L) denotes the volume of the metal solution, C_t (mg/L) is the metal ion concentration at any time, and M (g) is the quantity of TSB.

Results and Discussion:

1. Biochar Yield:

The biochar yield (YP) from finger millet (*Eleusine coracana*) biomass was determined using Equation (1). Based on the initial raw biomass mass (m_R) and the mass of biochar obtained after pyrolysis (m_B), the calculated yield was 38 %. This yield reflects the efficiency of conversion under oxygen-limited pyrolysis at 400 °C with a heating rate of 20 °C min^{-1}. At this moderate temperature, substantial thermal degradation of hemicellulose and cellulose occurs, while partial lignin retention contributes to the residual solid mass.

2. FTIR :

FTIR analysis confirmed successful Methylene Blue (MB) adsorption onto biochar, evidenced by notable spectral changes. Key functional groups identified before adsorption included hydroxyl (O-H, ~3400 cm^{-1}), aliphatic (C-H, ~2920 cm^{-1}), carbonyl/carboxylic (C=O, ~1650 cm^{-1}), and C-O (1000–1200 cm^{-1}) stretches. Post-adsorption, the diminished O-H peak and broadening of the C=O band indicated direct interactions between these groups and MB molecules. SEM imaging supported these findings, revealing a transition from highly porous, rough biochar surfaces to reduced porosity and smoother textures after dye uptake, consistent with pore filling. These observations align with previous literature (Nguyen et al., 2022; Behloul et al., 2022; Jeganathan et al., 2024), which emphasize the importance of porosity, surface functional groups, and activation processes in enhancing adsorption. The results collectively suggest that adsorption mechanisms involve hydrogen bonding, electrostatic attraction, and π-π stacking between MB and the biochar's surface functional groups, underpinning the material's effectiveness in dye removal.

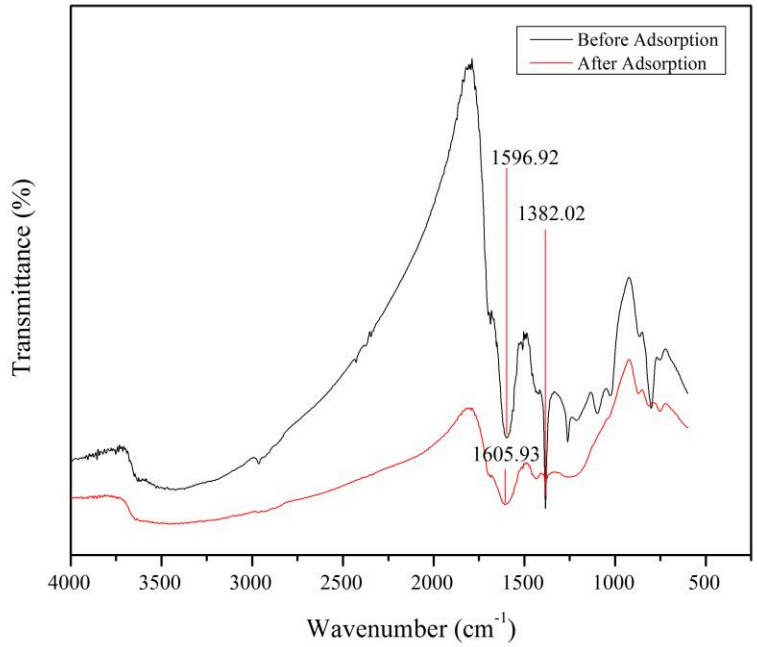

Figure 1: FTIR spectra of biochar illustrating structural and functional group changes before and after dye adsorption

Biochar before adsorption is showing characteristic functional groups including hydroxyl, carbonyl, and ether groups. Biochar after adsorption of Methylene Blue (MB), revealing spectral modifications associated with aromatic and amine group interactions.

3. PSA

Particle size analysis (PSA) revealed that biochar exhibited a uniform nanoscale distribution prior to adsorption, with a size starting from 12.8 nm, indicating a highly dispersed material with significant surface area suitable for adsorption. After Methylene Blue (MB) adsorption, the particle size starting from 0.7 nm, suggesting strong interactions between the dye molecules and the biochar surface. This reduction likely results from electrostatic attraction, π–π stacking, and pore filling, which may lead to partial compaction or restructuring of the biochar matrix. Such trends are consistent with previous findings (Bakhsh et al., 2022), which highlight the impact of nanoscale properties on adsorption efficiency. The decreased particle size after adsorption not only reflects robust dye–biochar interfacial interactions but also supports enhanced adsorption

efficiency due to increased surface-to-volume ratio. Comparative analyses with other dyes, such as Malachite Green, further indicate that the extent of particle size reduction depends on the dye's molecular characteristics and adsorption mechanisms (Roy et al., 2020). These results affirm the structural adaptability and high functional capacity of finger millet biochar in dye removal applications, in line with literature emphasizing the crucial role of nanoscale physicochemical properties in adsorption systems.

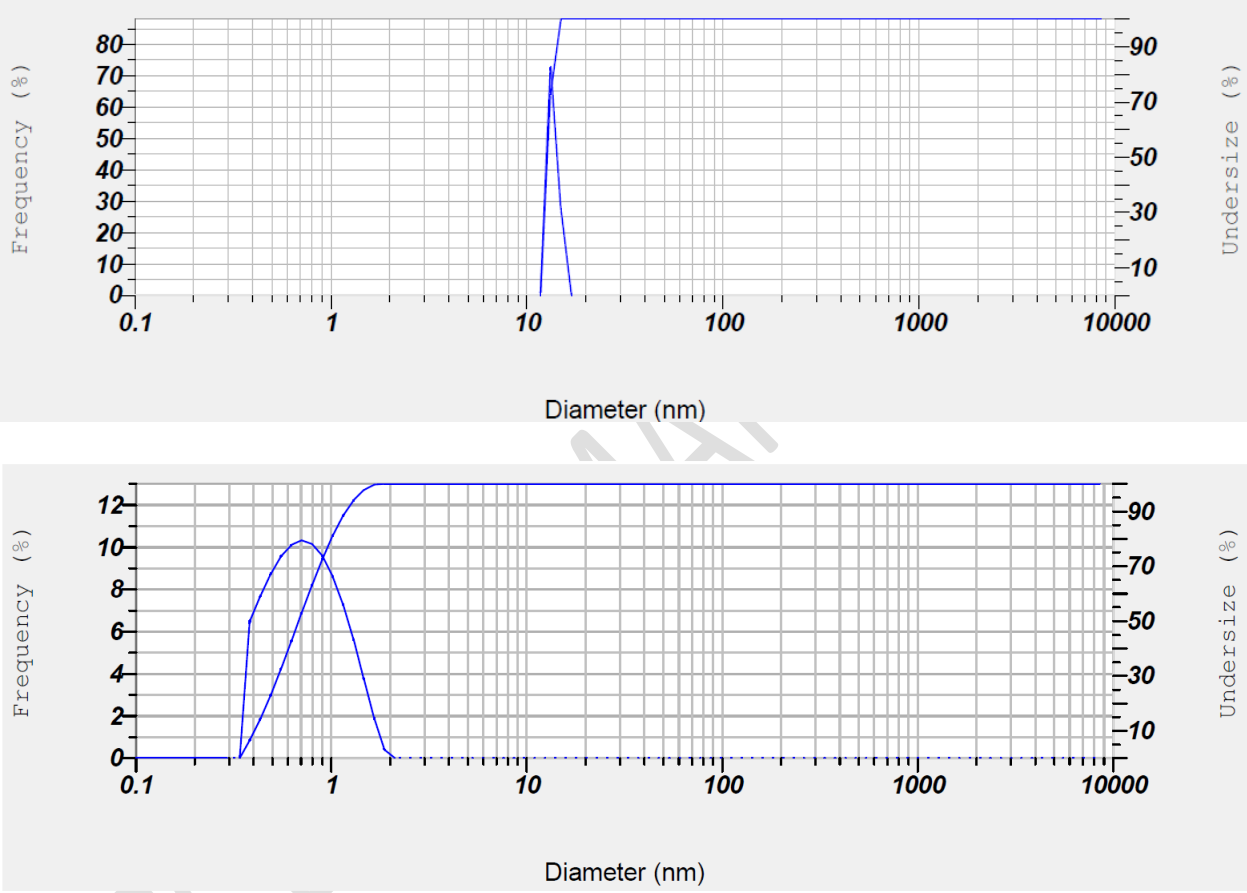

Figure 2: Particle size distribution of Biochar (a) Before adsorption (b) After adsorption of Methylene Blue (MB).

4. SEM EDX

SEM analysis revealed that biochar initially possessed a highly porous and rough surface, indicative of abundant active sites suitable for dye adsorption (Figure 3). After methylene blue (MB) uptake, the biochar surface appeared more compact and smoother, signifying effective pore filling and strong dye–biochar interactions. These morphological changes are consistent

with previous studies (Chellappan et al., 2023) that attribute enhanced adsorption to the presence of surface functional groups, such as hydroxyl and carboxylic groups, which facilitate hydrogen bonding and electrostatic interactions. Complementary EDX analysis confirmed shifts in elemental composition after adsorption, suggesting modifications in surface charge and reactivity. Collectively, these results highlight the critical role of surface morphology and chemistry in governing adsorption efficiency, and they underscore the sustainable potential of biochar from diverse biomass sources for effective dye removal, as supported by existing literature (Lalay et al., 2021; Singh et al., 2022; Srivastava et al., 2020).

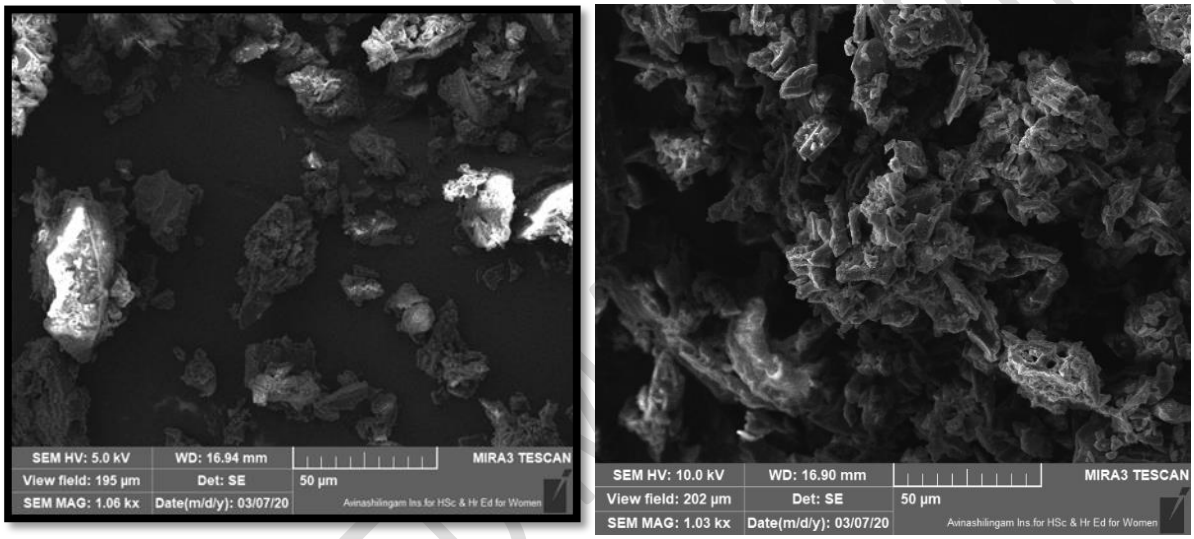

Figure 3: SEM images illustrating the surface morphology of biochar before and after dye adsorption.

Biochar before adsorption, showing a porous and rough surface with numerous active sites suitable for adsorptionAfter adsorption of Methylene Blue (MB), biochar reveals an even smoother and more compact surface, indicating extensive pore filling and strong interaction between the dye and the biochar surface.

5. ZETA

Zeta potential analysis in the current study confirmed that biochar's surface charge effectively interacts with cationic and anionic dyes. The near-neutral zeta potential of the biochar prior to adsorption indicates the presence of a weak surface charge (Figure 4a). This observation aligns with the perspective of (Xia et al. 2023), suggesting that the surface charge of biochar

dynamically changes under varying pH conditions. Following the adsorption of Methylene Blue (MB), the increased positive zeta potential supports the findings reported by (Ge et al., 2023), indicating that the adsorption of cationic dyes is more effectively achieved through electrostatic attraction with negatively charged surface groups (Figure 4b). The importance of functional groups, such as hydroxyl and carboxyl groups, in enhancing these interactions emphasises the roles of hydrogen bonding and electrostatic interactions (Hou et al., 2022). This reinforces the multipurpose nature of biochar, demonstrating its adaptability for the adsorption of diverse dye types while optimizing dye removal applications and adsorption processes (Li, 2023).

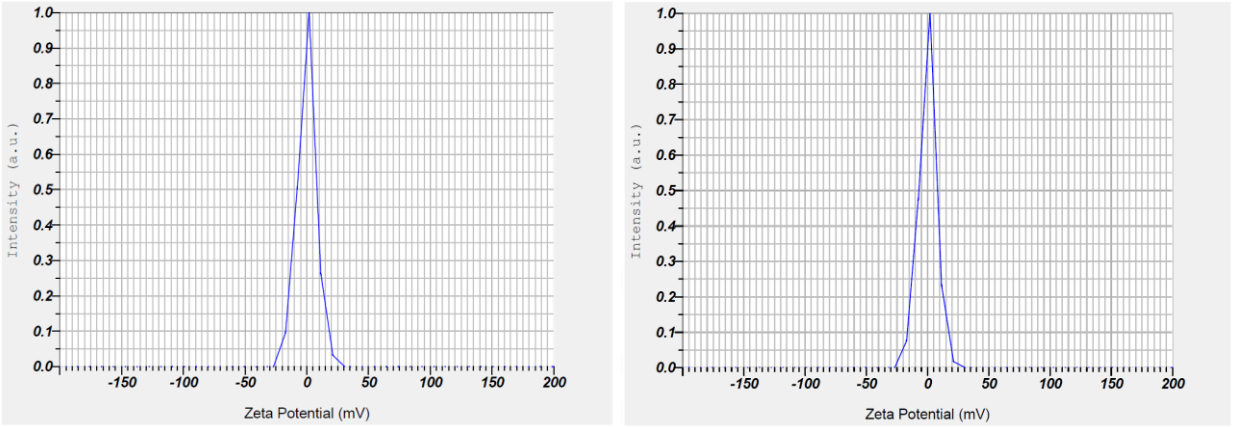

Figure 4: Zeta potential analysis of biochar before and after dye adsorption

Before adsorption, the biochar exhibited a near-neutral surface charge, indicating its potential versatility for adsorbing both cationic and anionic dyes. After Methylene Blue (MB) adsorption, the biochar showed a shift towards a positive zeta potential, confirming the strong attachment of cationic dye molecules onto its surface.

6. Effect of pH on dye removal

The results (Figure 5) demonstrate that Methylene Blue (MB) removal efficiency is highly dependent on both solution pH and adsorbent dosage. Maximum adsorption (\~100%) occurred at neutral to slightly alkaline pH (7–8), where electrostatic attraction between the cationic dye and the negatively charged biochar surface is strongest. Increasing the biochar dosage enhanced dye removal up to an optimal value of 1 g/L, beyond which efficiency plateaued, indicating site saturation—a trend consistent with previous reports (Yu et al., 2018). At lower dosages, MB removal was still effective due to favorable surface interactions, but further increases in dosage

did not significantly improve efficiency, echoing the behavior noted by Chen et al. (2012) and Fang (2012). These findings underscore the importance of optimizing pH and adsorbent dosage to maximize dye removal while ensuring efficient use of resources, as highlighted in related literature (Singh et al., 2022).

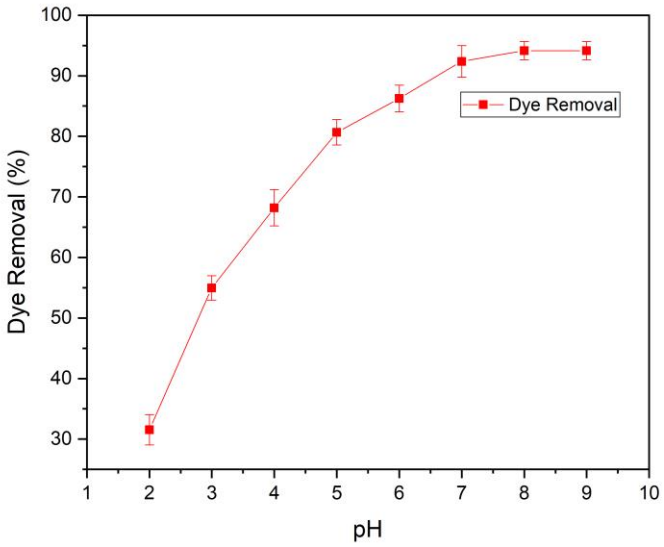

Figure 5: Effect of pH on toxic dye adsorption

Effect of adsorbent dosage on dye removal

The influence of adsorbent dosage on dye removal efficiency is evident from the results, as shown in Figure 6, where the percentage removal of Methylene Blue (MB) increased with dosage, reaching a plateau at approximately 1 g/L. At lower dosages, MB exhibited higher removal efficiency (~100%) at 1–1.5 g/L. Beyond 1 g/L, the additional dosage did not significantly improve the efficiency, indicating saturation of the available adsorption sites. This trend aligns with the studies by Yac'Cob et al. (2016), which attributed similar behaviors to increased active sites at higher dosages, followed by site saturation and reduced dye concentration gradients. The advantage in MB adsorption efficiency at lower dosages can be attributed to the stronger electrostatic interactions between the cationic dye and the negatively charged biochar surface (Fang, 2012). The results confirm that 1 g/L is the optimal dosage for effective dye removal, balancing the maximum efficiency with resource use (Bagheri & Mardani, 2019).

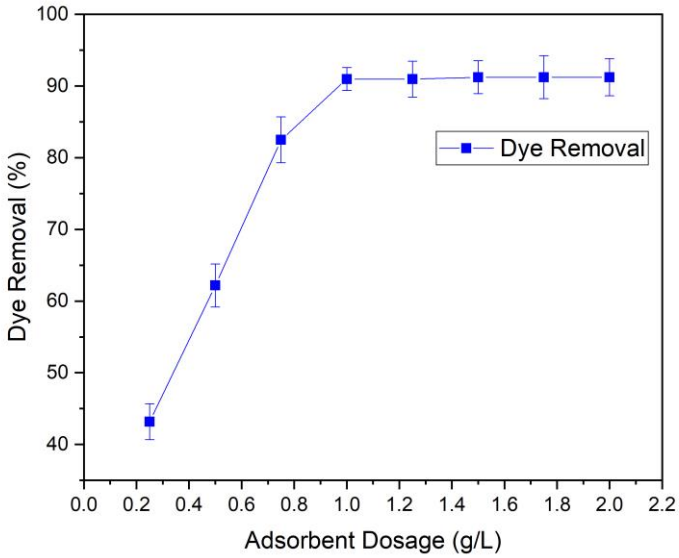

Figure 6: Effect of adsorbent dosage on toxic dye adsorption

Effect of dye concentration

The relationship between the initial dye concentration and removal efficiency for Methylene Blue (MB) using biochar demonstrated that the adsorption efficiency decreased as the dye concentration increased, as shown in Figure 7. MB achieved high removal efficiencies at lower concentrations (50–100 mg/L), reaching ~100%. At 300 mg/L, removal rates dropped to ~60% for MB. It has been observed that an increase in concentration has led to saturation provided by adsorption sites on activated biochar surface (Kumar et al.., 2021). At lower concentrations, the ratio between active sites and dye molecules favorably enhanced the adsorption efficiency, while at higher concentrations, competitive adsorption with site saturation as per Langmuir and Freundlich isotherm becomes the most feasible (Singh et al., 2022). MB, a cationic dye, shows specific behaviors from the difference in electrostatic interaction between the biochar surface and MB dyes (Chen et al.,2012). Present laboratory studies underscore the efficacy of biochar at relatively lower dye concentrations and accentuate the importance of checking for optimum initial dye concentration to maximize removal potential without concomitantly saturating the available sites.

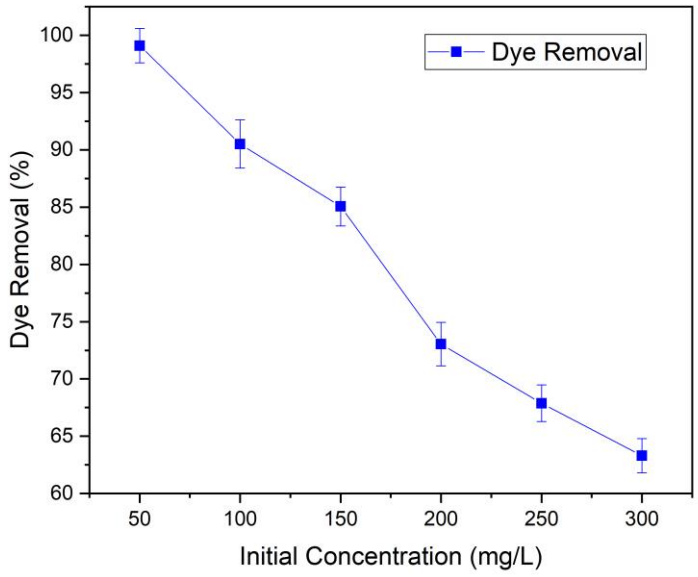

Figure 7: Effect of initial dye concentrations on toxic dye adsorption

Effect of contact time:

One observation from the Methylene Blue (mb) case is that its removal is easier when concentrations are low, particularly at 100 mg/L or less. For example, biochar achieves high removal rates quickly, reaching equilibrium in about 60 minutes (Figure 8). Although removal rates are significantly high- nearly 100%- in the 50–100 mg/L range, its removal efficiency declines at concentrations exceeding 200–250 mg/L due to saturation of the available active sites on the biochar. Initially, rapid adsorption occurs because of a steep concentration gradient and numerous active sites, but this slows down as equilibrium is approached (Yu et al., 2018). This behaviour is often modelled by the pseudo-second-order kinetic model, suggesting that chemical interactions play a key role in the adsorption process (Hanoon & Ahmed, 2019; Habila et al., 2023). The effectiveness of MB across all concentrations can be linked to its cationic nature, which enhances electrostatic interactions with the negatively charged surface of biochar (Chen et al., 2012). Therefore, 60 minutes is adequate for optimal adsorption of both dyes, with MB showing superior performance, especially at higher concentrations.

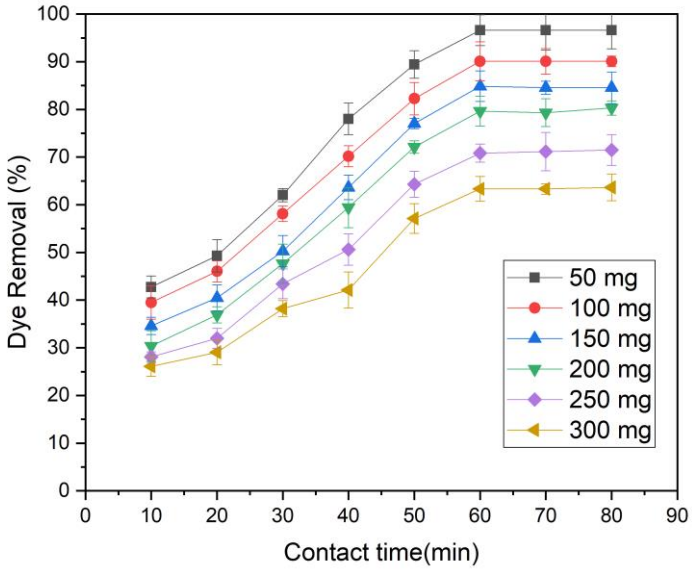

Figure 8: Effect of contact time on Methylene Blue dye adsorption

Effect of temperature on adsorption efficiency:

The effect of temperature on the adsorption of Methylene Blue (MB) demonstrates an endothermic process, with adsorption efficiencies increasing moderately as the temperature increased (Figures 9). At lower concentrations (50–100 mg/L), MB achieved nearly 100% removal efficiency. However, at higher concentrations (200–300 mg/L), the adsorption efficiency declined slightly, owing to the saturation of the active sites. The optimal temperature for both dyes was 330 K, where maximum adsorption was observed across all concentrations. Improved adsorption occurs with increased temperature owing to enhanced molecular diffusion and active site availability. The superiority of MB at all concentrations can be attributed to the stronger electrostatic attraction between cationic dye and negatively charged biochar (Chen et al., 2012). The structure of biochar produced at higher temperatures has affected its adsorption properties thus also supporting the endothermic nature of the adsorption process (Mahdi, 2023). These result warrant the benefits of the dye-biochar interaction conditions that by increasing the temperature in response to the decrease in power from the adsorption efficiency with increased dye concentrations.

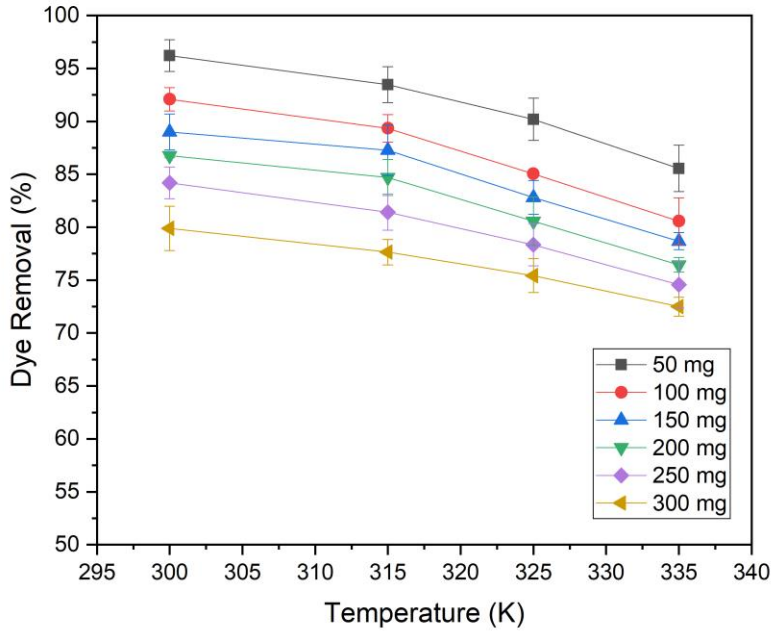

Figure 9: Effect of temperature on Methylene Blue dye adsorption

Adsorption Isotherms:

Freundlich isotherms suggest adsorption occurs on heterogeneous surfaces with non-uniform adsorption energies (Karthik et al., 2020). Freundlich's nonlinear equation for isothermal systems is as equation 4 as given below:

$$q_e = K_f C_e^{1/n} \quad (4)$$

The adsorption intensity is given by n, and the Freundlich constant is given by K_f (mg/g).

The Langmuir isotherm states that all adsorption sites on a monolayer surface have the same energy. Adsorption isotherms provide constants and equilibrium adsorption capacities, which show surface characteristics and adsorbent affinity (Karthik et al., 2020). Langmuir's non-linear equation is given as equation 5.

$$q_e = \frac{q_m K_L C_e}{1 + K_L C_e} \quad (5)$$

As with any isotherm, Langmuir's K_L is the Langmuir isotherm constant (L/mg), whereas q_m is the maximum monolayer capacity (mg/g). From q_e vs. C_e plots at different temperatures (20, 30, 40, and 50 °C), K_L and q_m values were calculated.

The Fritz-Schlunder model combines Langmuir and Freundlich isotherms to more accurately describe adsorption on heterogeneous surfaces with both monolayer and multilayer characteristics and is expressed using equation 6 as below:

$$q_e = K_{FS} * q_m * C_e^{\alpha} / (1 + K_{FS} * C_e^{\alpha}) \quad (6)$$

Here, q_e represents the amount of adsorbate adsorbed at equilibrium, C_e is the equilibrium concentration of the adsorbate, q_m is the maximum adsorption capacity, and K_{FS} is the Fritz-Schlunder model constant.

The Radke-Prausnitz isotherm is favored at low adsorbate concentrations because it effectively captures the heterogeneous nature of adsorption sites, providing a more accurate model where specific sites are preferentially occupied, unlike simpler models. It is represented using the following equation 7.

$$q_e = q_m * (K_{RP} * C_e)^{mRP} / (1 + (K_{RP} * C_e)^{mRP}) \quad (7)$$

q_e is the amount of adsorbate adsorbed per unit mass of adsorbent at equilibrium, q_m is the maximum adsorption capacity of the adsorbent, K_{RP} is the equilibrium constant related to the adsorption affinity, C_e is the equilibrium concentration of the adsorbate in the solution and m_{RP} is the model exponent, which is a dimensionless parameter that characterizes the heterogeneity of the adsorption sites.

Table 1. Adsorption isotherm parameters for the removal of Methylene Blue onto Finger millet biochar

Removal of Methylene Blue dye onto finger millet biochar					
S. No.	**Isotherm models**	**Parameters**	**R^2**	**SSE**	**RMSE**
1	Langmuir	q_m = 191.8 (mg/g) K_L= 0.0999 (L/mg)	0.8504	2.03	16.5
2	Freundlich	K_F= 53.56 ((mg/g)(L/mg)$^{(1/n)}$), n = 3.77 (g/L)	0.9877	1.67	6.47
3	Fritz-Schlunder	q_{mFS} = 6.987 K_{FS} = 25	0.817	2.48	18.8

		$\alpha = 0.55$			
4	Radke-Prausnitz	$q_{mRP} = 53.16$ (mg/g), $K_{RP} = 2$ mRP = 0.7694	0.9634	1.98	12.89

In addition to the widely recognized Langmuir and Freundlich isotherm models, the Fritz–Schlunder and Radke–Prausnitz models were employed to elucidate the complex adsorption behavior of Methylene Blue onto finger millet biochar. The Fritz–Schlunder model, characterized by four adjustable parameters, presents enhanced flexibility in fitting empirical data across heterogeneous and multilayer adsorption systems. This adaptability is particularly relevant considering the heterogeneous surface morphology observed via scanning electron microscopy (SEM). The Radke–Prausnitz model integrates aspects of both the Langmuir and Freundlich models, effectively accommodating saturation phenomena at elevated concentrations while addressing surface heterogeneity at lower concentrations. The statistical performance metrics of the Radke–Prausnitz model ($R^2 = 0.9634$, RMSE = 12.89) further substantiate its applicability and accuracy in characterizing this adsorption system, outperforming the traditional Langmuir model.

While Freundlich showed the best overall fit ($R^2 = 0.9877$), the inclusion of these extended models aids in a more nuanced interpretation of adsorption mechanisms, consistent with FTIR and SEM findings.

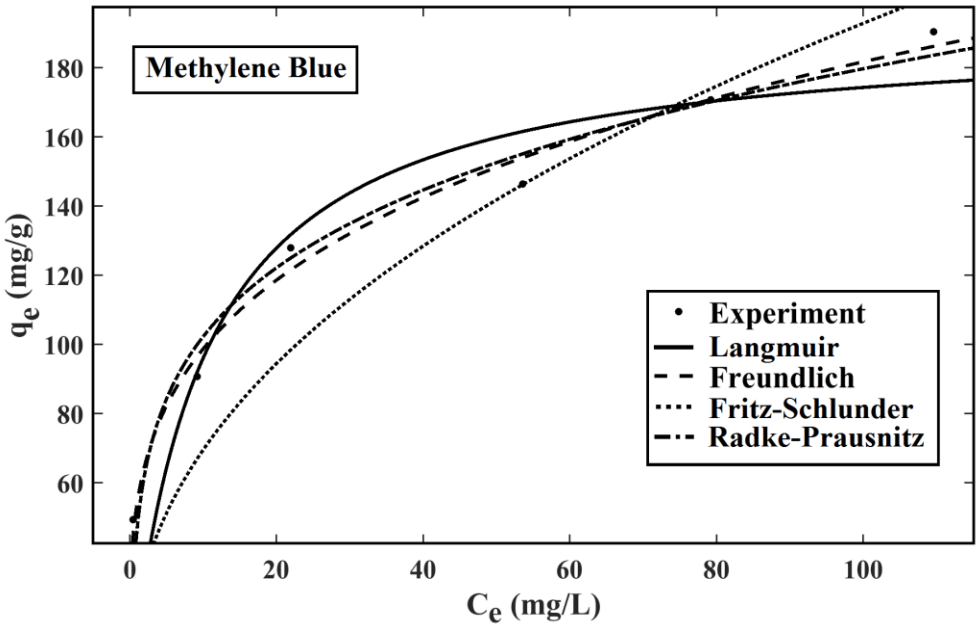

Figure 10: Isotherm study Methylene Blue dye adsorption

Adsorption Isotherm Analysis of Methylene Blue onto Finger Millet Biochar

Four isotherm models, Freundlich, Fritz-Schlunder, and Radke-Prausnitz, were employed in the adsorption of Methylene Blue on finger millet biochar to determine the most fitting model for their parameters and statistical accuracies (Table 1). Of these, the Freundlich equation fitted the best as it showed the highest coefficient of correlation of 0.9877 and, hence, the smallest SSE (1.67) and smallest RMSE (6.47). The Freundlich parameters (K_F = 53.56 mg/g)(L/mg) $^{1/n}$), (n = 3.77) indicate a heterogeneous surface property for multilayer adsorption. This suggests the presence of multiple adsorption sites with different affinities and interaction possibilities between them (Nie,2024).

Langmuir model was found to fit between Freundlich and the Fritz-Schlunder model in between and thus offers a moderate fit (R^2 = 0.8504) with the highest q_m = 191.8 mg/g. K_L = 0.0999 L/mg signifies a moderate interaction strength between the Methylene Blue adsorbate and the adsorbent. However, the model showed much larger error measurement values (SSE = 2.03, RMSE = 16.5) than the better-fitting Freundlich model due to the lack of capturing surface heterogeneity and multilayer adsorption phenomenon.

The Radke-Prausnitz model has a good fit (R^2 = 0.9634) and moderate error values (SSE = 1.98, RMSE = 12.89). The parameters q_{mRP} = 53.16mg/g, K_{RP} = 2 and m_{RP} = 0.7694 support the

possibility of a two-mode mechanism-integrated homogeneous and multiple-layer processes. Thus, an M-blanket model may reflect a balanced approach to displeasing adsorption behavior. The Fritz-Schlunder performed worst with the lowest R^2 = 0.817 and highest error metrics (SSE = 2.48, RMSE = 18.8). Near failure in description suggests the model is ill-suited to portraying the adsorption of Methylene Blue on the finger millet biochar surface, calling into question its credibility in part. The poor prediction capability indicates that the model's assumptions do not accurately project the experimental adsorption behavior.

The Freundlich model is the one that is best suited to describe the adsorption process, which requires due consideration for surface heterogeneity and the mechanism of multilayer adsorption. This supports isothermal studies on the adsorption of antibiotics and heavy metals in biochar materials, where multilayer adsorption and material heterogeneity are the prominent mechanisms (Xie et al., 2023). Upon validation, the lack of a good fit for the model places a potent basis for understanding other materials' complex adsorption processes. The former further suggests that the model's hypothetical assumptions may not accommodate the actual experimental conditions, hence limiting the model's predictive capacity. Moreover, the moderate fit of the Langmuir isotherm supports the single-layer adsorption mechanism, mainly at the high concentration of MB. In contrast, the adaptability of Radke-Prausnitz suggests possible cooperative adsorption or surface rearrangement processes. The information from these studies could be beneficial in optimising adsorption systems for the removal of dyes from aqueous solutions, thus overriding the significance of surface chemistry and morphological corrugation within the adsorption process (Khan et al., 2022; Li et al., 2023).

Adsorption Kinetics:

When solute concentrations are low, the pseudo-first-order kinetic model is preferable (Saravanan et al., 2021). The pseudo-first-order kinetic model equation is given by equation 7.

$$q_t = q_e(1 - exp(-k_1 t)) \quad (7)$$

The pseudo-second-order kinetic model is preferred for adsorption processes as it typically offers a better fit to experimental data and it is directly linked to the adsorption capacity at equilibrium. The kinetic model is represented in equation 8 as below:

$$t/q_t = 1/(K_2 q_e^2) + t/q_e \quad (8)$$

q_t is the amount adsorbed at time t, q_e is the amount adsorbed at equilibrium, and k_2 is the pseudo-second-order rate constant.

The Elovich equation, used to describe chemisorption kinetics, relates the amount of substance adsorbed (q_t) to time (t) using two parameters: α_E (initial adsorption rate) and β_E (desorption constant) as given in equation 9.

$$q_t = (1/\beta_E)\ln(\alpha_E\beta_E) + (1/\beta_E)\ln(t) \quad (9)$$

This study examined the adsorption kinetics of Methylene Blue dye through pseudo-first-order, pseudo-second-order, and Elovich kinetic models at initial concentrations (C_0) between 50 and 300 mg/L (Table 2). With an increase in initial concentration, the equilibrium adsorption capacities (q_e) rise from 49.65 mg/g at 50 mg/L to 194.28 mg/g at 300 mg/L. The kinetic models demonstrate a satisfactory fit, with R^2 values ranging from 0.9462 to 0.9659. However, there is a tendency to underestimate the qe values, particularly at elevated concentrations, with q_e values varying from 50.3 mg/g at 50 mg/L to 230.4 mg/g at 300 mg/L. The pseudo-second-order model exhibits an R^2 value ranging from 0.9197 to 0.9332, indicating a marginally weaker overall fit. At elevated concentrations, it tends to overestimate q_e values ranging from 60.47 mg/g at 50 mg/L to 293.8 mg/g at 300 mg/L. Furthermore, the K_2 values diminish as concentrations rise; for instance, at 50 mg/L, K_2 equals 0.0012 g/mg/min, whereas at 300 mg/L, K_2 equals 0.0002 g/mg/min. The adsorption of Methylene Blue may not be sufficiently represented by the Elovich model, as indicated by R^2 values between 0.8821 and 0.8898. As concentration increases, E values decrease; however, the adsorption rate and surface coverage vary, increasing E values. The pseudo-first-order model offers a more accurate representation of experimental q_e values, especially at lower concentrations, indicating its greater relevance in describing the adsorption dynamics of Methylene Blue on finger millet biochar compared to the pseudo-second-order model. The Elovich model, characterised by a relatively low R^2, fails to represent this system's kinetics adequately.

A kinetic study using jackfruit peel biochar at initial Methylene Blue concentrations of ~24–41 mg/L found that the Elovich model provided the best fit, outperforming both pseudo-first- and pseudo-second-order models—indicating a dominant chemisorptive but heterogeneous adsorption mechanism (Ton-That et al., 2023). For Methylene Blue adsorption on biomass from the alga *Desmarestia antarctica*, the pseudo-second-order model showed an excellent fit across

initial concentrations ranging from 25 to 200 mg/L, with all R^2 values exceeding 0.95. This suggests that chemisorption and possibly multi-step mechanisms like film diffusion and intraparticle diffusion contribute significantly. Notably, the system achieved a remarkably high equilibrium adsorption capacity (q_e = 702.9 mg/g) at 25 °C, with an initial concentration range of 25–1400 mg/L and an equilibrium time of 540 min (Guarín et al., 2018).

Table 2. Adsorption kinetic parameters for removing toxic dyes Methylene Blue onto finger millet.

Removal of Methylene Blue dye onto Finger millet											
S. No.	**C_o (mg/L)**	**q_e (exp)**	**Pseudo first order**			**Pseudo second order**			**Elovich kinetics**		
			q_e (mg/g)	**k_1 (min^{-1})**	**R^2**	**q_e (mg/g)**	**K_2 (g/mg min)**	**R^2**	**α_E**	**β_E**	**R^2**
1	50	49.65	50.3	0.0612	0.9603	60.47	0.0012	0.9315	0.1319	4.789	0.8872
2	100	92.42	97.55	0.0566	0.9659	119.4	0.0005	0.9332	0.0417	11.12	0.8898
3	150	131.38	140.5	0.0541	0.9588	173.7	0.0003	0.9261	0.0229	17.19	0.8852
4	200	162.27	183.2	0.0479	0.9563	233.2	0.0002	0.9239	0.0103	25.46	0.8874
5	250	180.95	214.4	0.0472	0.9523	274.1	0.0002	0.9197	0.0882	30.44	0.8836
6	300	194.28	230.4	0.0473	0.9462	293.8	0.0002	0.9159	0.0079	32.42	0.8821

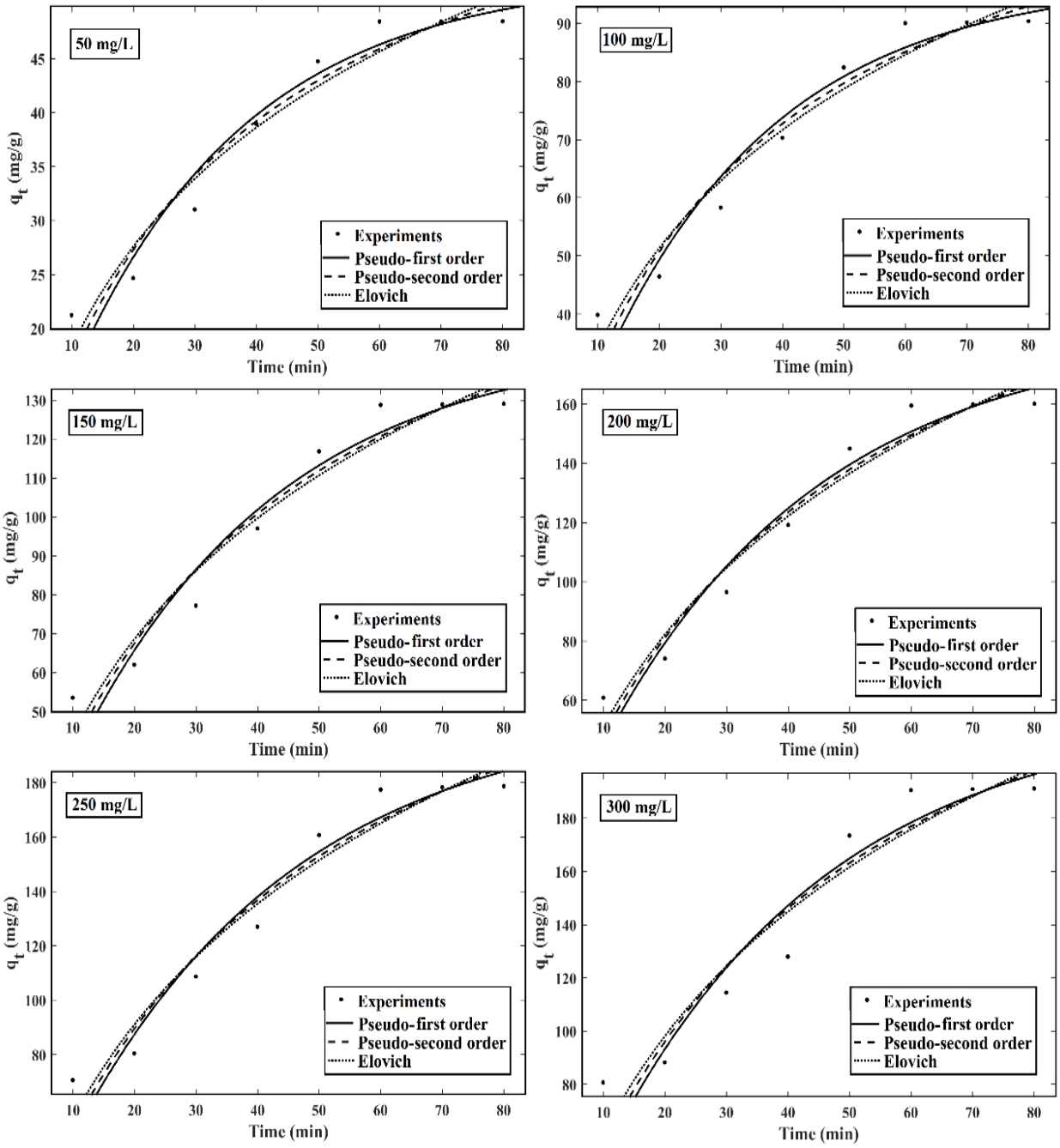

Figure 11: Adsorption kinetic parameters for the removal of toxic MB on to finger millet

Figure 11 illustrates the adsorption kinetics of Methylene Blue at different initial concentrations (50–300 mg/L) over time, analysed using three kinetic models: pseudo-first-order, pseudo-second-order, and Elovich. The experimental data aligns closely with both pseudo-first-order and pseudo-second-order models, with the pseudo-second-order model offering a marginally superior fit at elevated concentrations as it more accurately reflects the experimental trends. The Elovich model demonstrates reduced alignment, especially at elevated concentrations. The data demonstrate that adsorption capacity rises with initial concentration, and the pseudo-second-order model most accurately characterizes the dynamics of the adsorption process.

Table 3. Thermodynamic parameters for the removal of toxic dyes Methylene Blue onto finger millets

Removal of Methylene Blue dye onto finger millet						
C_o(mg/L)	ΔH^o (kJ mol^{-1})	ΔS^o (J mol^{-1})	ΔG^o (kJ mol^{-1})			
			303 K	313 K	323 K	333 K
50	-43.6957	-116. 095	-8.63	-7.1881	-6.1707	-5.1165
100	-30.3808	-71.1792	-6.3507	-5.6862	-4.739	-4.0253
150	-24.315	-61.5619	-5.5435	-5.237	-4.4232	-3.7472
200	-21.2074	-53.5699	-4.8974	-4.5632	-3.9061	-3.3203
250	-17.6556	-44.1016	-4.2131	-3.9389	-3.4905	-2.8786
300	-11.9934	-27.8591	-3.5382	-3.2724	-3.0427	-2.6825

The thermodynamic parameters for the adsorption of Methylene Blue onto finger millet biochar suggest that the process is both spontaneous and exothermic (Table 03). The negative enthalpy change values (ΔH◦) observed across all concentrations, which range from- 43. 6957 kJ/mol to-11. 9934 kJ/mol, indicate that the adsorption process is exothermic as it releases heat. The negative entropy change (ΔS) values, ranging from- 116. 095 J/mol to-27. 8591 J/mol, indicate a reduction in randomness at the solid- liquid interface during the adsorption process. The Gibbs free energy change (ΔG◦) values remain negative across all temperatures (303 K to 333 K) and initial concentrations, thereby confirming the spontaneous nature of the adsorption process. However, the (ΔG◦) values become less negative with rising temperature, suggesting that elevated temperatures diminish the spontaneity of the process, which aligns with the characteristics of an exothermic reaction. Lower concentrations (e. g., 50 mg/l) demonstrate greater spontaneity (ΔG◦) at 303 K =- 8. 63 kJ/mol, whereas higher concentrations (e. g., 300 mg/l) indicate diminished spontaneity (ΔG◦) at 303 K =- 3. 5382 kJ/mol. A decrease in ΔG with

increasing temperature is often observed, indicating that higher temperatures favor the adsorption process. Gopinathan et al. (2016) observed that the fall in ΔG values, due to the accompanying increase in temperature, seems to indicate that the adsorption of Orange G dye is increasingly favorable at the higher temperature, providing evidence of the exothermic nature of the process. Jayachandran et al. (2021) found that BG 4 and AF adsorption on activated carbon is spontaneous and exothermic, with decreasing ΔG values as the temperature rises. Zhang et al. (2022) further showed spontaneous Congo Red and Methylene Blue adsorption on activated carbons, suggesting strong adsorbent/dye interactions. The negative value of ΔG results from an increase in temperature, which raises ΔS, while there is a negative association between ΔG and ΔH shows that the reaction is feasible in room temperature. Sampranpiboon et al. (2014) stated in their discussion that when a process of adsorption is spontaneous, the ΔG values will be negative. This result is due to the exothermic change in enthalpy and an increase in entropy. In another study, the adsorption of Methylene Blue on modified nanocellulose was concluded to be spontaneous by negative ΔG values, implying favorable absorption conditions (Kara et al., 2021). The data shows that adsorption efficiency decreases as dye concentration increases and temperature rises. The adsorption process is thermodynamically beneficial, though it is clearly influenced by concentration and temperature.

Conclusion:

The present study demonstrates that biochar derived from finger millet (*Eleusine coracana*) waste is an effective, low-cost, and eco-friendly adsorbent for the removal of Methylene Blue dye from water. The adsorption process followed the Freundlich isotherm model, indicating multilayer adsorption on a heterogeneous surface, while kinetic studies revealed a pseudo-second-order mechanism, suggesting chemisorption as the primary mode of interaction. Thermodynamic parameters further confirmed that the adsorption is spontaneous and exothermic, although spontaneity decreases at higher temperatures. Structural and chemical analyses using SEM, FTIR, PSA, and Zeta potential evidenced the presence of a porous structure and active functional groups, as well as changes in surface charge after dye adsorption, supporting the involvement of electrostatic and π–π interactions. The high adsorption capacity (up to 191.8 mg/g) highlights the potential of finger millet biochar for efficient dye remediation. These findings align with the study's objectives by confirming the material's adsorption

performance and mechanistic pathways. For broader practical application, future research should explore the biochar's effectiveness in real wastewater, continuous flow systems, and repeated regeneration cycles, alongside comprehensive techno-economic and life cycle assessments. Overall, the results position finger millet biochar as a promising and sustainable adsorbent for large-scale water treatment, warranting further validation under real-world operational conditions.

Reference:

1. Akhtar, M. S., Ali, S., & Zaman, W. (2024). Innovative Adsorbents for Pollutant Removal: Exploring the Latest Research and Applications. *Molecules*, **29(18)**, 4317.
2. Bagheri, K. M., & Mardani, E. (2019). Removal of acid orange 7 dye from aqueous solutions using polyaniline-modified rice bran: isotherms, kinetics, and thermodynamics. *Environmental Health Engineering and Management*, **6(3)**, 203–213.
3. Bakhsh, E., Bilal, M., Ali, M., Ali, J., Wahab, A., Akhtar, K., & Khan, S. (2022). Synthesis of activated carbon from *Trachycarpus fortunei* seeds to remove cationic and anionic dyes. *Materials*, **15(6)**, 1986.
4. Batagarawa, S. M., & Ajibola, A. K. (2019). Comparative evaluation for the adsorption of toxic heavy metals onto millet, corn and rice husks as adsorbents. *Journal of Analytical & Pharmaceutical Research*, **8(3)**, 119–125.
5. Behloul, H., Ferkous, H., Bougdah, N., Djellali, S., Alam, M., Djilani, C., & Benguerba, Y. (2022). New insights on CI-Reactive Red 141 dye adsorption using activated carbon prepared from the ZnCl2-treated waste cotton fibers: Statistical physics, DFT, COSMO-RS, and AIM studies. *Journal of Molecular Liquids*, **364**, 119956
6. Chellappan, S., Kallingal, A., Sajith, V., Nair, V., & Chinglenthoiba, C. (2023). Methyl orange dye adsorbed biochar as a potential Brønsted acid catalyst for microwave-assisted biodiesel production. *Environmental Science and Pollution Research*, **30(60)**, 125158–125164.
7. Chen, P., Lu, X., & Qiu, J. (2012). Study on adsorption properties of different dyes on montmorillonite. *Advanced Materials Research*, **454**, 305–309.
8. Fang, R. (2012). Preparation of corncob-based bio-char and its application in removing basic dyes from aqueous solution. *Advanced Materials Research*, 550–553, 2420–2423.
9. Ge, Q., Peng, L., Liu, M., Xiao, G., Xiao, Z., Mao, J., & Gai, X. (2023). Removal of methylene blue by porous biochar obtained by KOH activation from bamboo biochar. *Bioresources and Bioprocessing*, **10(51)**.
10. Gopinathan, R., Bhowal, A., & Garlapati, C. (2016). Adsorption characteristics of activated carbon for the reclamation of colored effluents containing Orange G and new solid–liquid phase equilibrium model. *Journal of Chemical & Engineering Data*, **62(1)**, 558–567.
11. Guarín, J. R., Moreno-Piraján, J. C., & Giraldo, L. (2018). Kinetic study of the bioadsorption of methylene blue on the surface of the biomass obtained from the algae *D. antarctica*. *Journal of Chemistry*, 2018, 2124845.

12. Habila, M., Moshab, M., El-Toni, A., AlOthman, Z., & Ahmed, A. (2023). Thermal fabrication of magnetic Fe3O4 (nanoparticle) carbon sheets from waste resources for the adsorption of dyes: kinetic, equilibrium, and UV–Visible spectroscopy investigations. *Nanomaterials*, **13(7)**, 1266.
13. Hanoon, M., & Ahmed, M. (2019). Adsorption of methyl orange from wastewater by using biochar. *Iraqi Journal of Chemical and Petroleum Engineering*, **20(3)**, 23–29.
14. Hou, J., Yu, J., Li, W., He, X., & Li, X. (2022). The effects of chemical oxidation and high-temperature reduction on surface functional groups and the adsorption performance of biochar for sulfamethoxazole adsorption. *Agronomy*, **12(2)**, 510.
15. Islam, M., & Mostafa, M. (2019). Textile dyeing effluents and environment concerns – a review. *Journal of Environmental Science and Natural Resources*, **11(1–2)**, 131–144.
16. Jayachandran, S., Sampath, K., & Kesavasamy, R. (2021). Experimental investigations on adsorption of reactive toxic dyes using *Hedyotis umbellata* activated carbon. *Adsorption Science & Technology*, 2021.
17. Jeganathan, Y., Asharp, T., & Nadarajah, K. (2024). Adsorptive behavior of engineered biochar/hydrochar for tetracycline removal from synthetic wastewater. *Environmental Pollution*, **345**, 123452.
18. Kara, H., Anshebo, S., Sabir, F., & Workineh, G. (2021). Removal of methylene blue dye from wastewater using periodiated modified nanocellulose. *International Journal of Chemical Engineering*, 2021, 1–16.
19. Karthik, V., Selvakumar, P., Sivarajasekar, N., Megavarshini, P., Brinda, N., Kiruthika, J., Balasubramani, K., Ahamad, T., & Naushad, M. (2020). Comparative and equilibrium studies on anionic and cationic dyes removal by nano-alumina-doped catechol formaldehyde composite. *Journal of Chemistry*, 2020.
20. Khan, M., Shanableh, A., Elboughdiri, N., Lashari, M., Manzoor, S., Shahida, S., … & Rehman, A. (2022). Adsorption of methyl orange from an aqueous solution onto a BPPO-based anion exchange membrane. *ACS Omega*, **7(30)**, 26788–26799.
21. Kumar, K., Bharath, M., & Krishna, B. (2021). Adsorption kinetics of reactive dye using agricultural waste: banana stem. *Water Practice & Technology*, **17(1)**, 128–138.
22. Kumar, K., Kumar, R., Kaushal, S., Thakur, N., Umar, A., Akbar, S., … & Baskoutas, S. (2023). Biomass waste-derived carbon materials for sustainable remediation of polluted environments: A comprehensive review. *Chemosphere*, 140419.
23. Lalay, G., Ullah, S., & Ahmed, I. (2021). Physiological and biochemical responses of *Brassica napus L.* to drought induced stress by the application of biochar and plant growth promoting rhizobacteria. *Microscopy Research and Technique*, **85(4)**, 1267–1281.
24. Li, S. (2023). Canola meal-derived biochar for highly efficient dye removal and the impact of compression treatment on porous structure. *Journal of Chemical Technology & Biotechnology*, **99(1)**, 227–235.
25. Li, Y., Sui, X., Wang, X., & Ji, H. (2023). Comparison of adsorption performance for Cd(II) removal from aqueous solution using biochar derived from different types of carbon sources: aquatic plants, pine branches and peat. *Journal of Chemical Technology & Biotechnology*, **98(9)**, 2154–2167.
26. Lin, Y. (2022). Decolorization of textile dyes by edible white rot fungi. *Journal of Emerging Investigators*.

27. Macchi, S., Alsebai, Z., Watanabe, F., Ilyas, A., Atif, S., Viswanathan, T., … & Siraj, N. (2021). Phosphorus and nitrogen co-doped carbon derived from cigarette filter for adsorption of methylene blue dye from aqueous solution. *Research Square*.
28. Mahdi, E. (2023). Adsorption of crystal violet dye by biochar produced from sugarcane bagasse under different temperatures. *Passer Journal of Basic and Applied Sciences*, **5(2)**, 422–427.
29. Martis, L. J., Parushuram, N., & Sangappa, Y. (2022). Preparation, characterization, and methylene blue dye adsorption study of silk fibroin–graphene oxide nanocomposites. *Environmental Science: Advances*, **1(3)**, 285–296.
30. Mohd Hanafiah, Z., Wan Mohtar, W. H. M., Rohani, R., Fadzizi, M. F., Wan-Mohtar, W. A. A. Q. I., Sayed, K., Abdul Manan, T. S. B., & Indarto, A. (2024). Removal of pharmaceutical compounds from sewage effluent by the nanofiltration membrane. *Journal of Water Process Engineering*, **68**, 106320.
31. Nasrin, T., Saha, A., Mohanta, M., Chaity, A., Alam, M., Shawon, M., … & Haque, M. (2022). Reduction of toxic effects of textile dye, Basic Red-18 on tilapia fish by bioremediation with a novel bacterium, *Mangrovibacter yixingensis* strain AKS2 isolated from textile wastewater. *Annual Research & Review in Biology*, 12–29.
32. Nguyen, P. X. T., Ho, K. H., Do, N. H. N., Nguyen, C. T. X., Nguyen, H. M., Tran, K. A., … & Le, P. K. (2022). A comparative study on modification of aerogel-based biosorbents from coconut fibers to treat dye- and oil-contaminated water. *Materials Today Sustainability*, **19**, 100175.
33. Nie, W. (2024). Comparative study for propranolol adsorption on the biochars from different agricultural solid wastes. *Materials*, **17(12)**, 2793.
34. Raman, C., & Kanmani, S. (2018). Decolorization of mono azo dye and textile wastewater using nano iron particles. *Environmental Progress & Sustainable Energy*, 38(S1).
35. Roy, D., Sheam, M., Hasan, M., Saha, A., Roy, A., Haque, M., … & Biswas, S. (2020). Isolation and characterization of two bacterial strains from textile effluents having malachite green dye degradation ability. *bioRxiv*.
36. Salahshoori, I., Wang, Q., Nobre, M. A., Mohammadi, A. H., Dawi, E. A., & Khonakdar, H. A. (2024). Molecular simulation-based insights into dye pollutant adsorption: a perspective review. *Advances in Colloid and Interface Science*, 103281.
37. Sampranpiboon, P., Charnkeitkong, P., & Feng, X. (2014). Determination of thermodynamic parameters of zinc(II) adsorption on pulp waste as biosorbent. *Advanced Materials Research*, 931–932, 215–219.
38. Saravanan, A., Kumar, P. S., Vo, D. V. N., Jayasree, R., Hemavathy, R. R. V., Karthik, V., Karishma, S., Jeevanantham, S., Manivasagan, V., & George, C. S. (2021). Surface improved agro-based material for the effective separation of toxic Ni(II) ions from aquatic environment. *Chemosphere*, **283**, 131215.
39. Sarkar, S., Banerjee, A., Halder, U., Biswas, R., & Bandopadhyay, R. (2017). Degradation of synthetic azo dyes of textile industry: a sustainable approach using microbial enzymes. *Water Conservation Science and Engineering*, **2(4)**, 121–131.
40. Sayed, K., Wan Mohtar, W. H. M., Mohd Hanafiah, Z., Wan-Mohtar, W. A. A. Q. I., Abd Manan, T. S. B., & Mohamad Sharif, S. A. B. (2024). Simultaneous enhanced removal of pharmaceuticals and hormone from wastewaters using series combinations of

ultra-violet irradiation, bioremediation, and adsorption technologies. *Journal of Water Process Engineering*, **57**, 104589.
41. Singh, M., Ahsan, M., Pandey, V., Singh, A., Mishra, D., Tiwari, N., … & Khare, P. (2022). Comparative assessment for removal of anionic dye from water by different waste-derived biochar vis a vis reusability of generated sludge. *Biochar*, **4(1)**.
42. Ton-That, L., Huynh, T. N., Duong, B. N., Nguyen, D. K., Nguyen, N. A., Pham, V. H., Ho, T. H., & Dinh, V. P. (2023). Kinetic studies of the removal of methylene blue from aqueous solution by biochar derived from jackfruit peel. *Environmental Monitoring and Assessment*, **195(11)**, 1266.
43. Xia, S., Liang, S., Qin, Y., Chen, W., Xue, B., Zhang, B., & Xu, G. (2023). Significant improvement of adsorption for phosphate removal by lanthanum-loaded biochar. *ACS Omega*, **8(28)**, 24853–24864.
44. Xie, S., Wang, Y., Ma, C., Zhu, G., Wang, Y., & Li, C. (2023). Pyrolysis of antibiotic mycelial residue for biochar: Kinetic deconvolution, biochar properties, and heavy metal immobilization. *Journal of Environmental Management*, **328**, 116956.
45. Yac'cob, N., Ngadi, N., & Rahman, R. (2016). Preparation and characterization of textile sludge-based activated carbon for dyes removal. *Applied Mechanics and Materials*, **818**, 250–253.
46. Yaseen, D., & Scholz, M. (2018). Textile dye wastewater characteristics and constituents of synthetic effluents: a critical review. *International Journal of Environmental Science and Technology*, **16(2)**, 1193–1226.
47. Yu, J., Zhang, X., Wang, D., & Li, P. (2018). Adsorption of methyl orange dye onto biochar adsorbent prepared from chicken manure. *Water Science & Technology*, **77(5)**, 1303–1312.
48. Zhang, L., Yang, L., Chen, J., Yin, W., Zhang, Y., Zhou, Gao, F., & Zhao, J. (2022). Adsorption of Congo red and methylene blue onto nanopore-structured ashitaba waste and walnut shell-based activated carbons: statistical thermodynamic investigations, pore size and site energy distribution studies. *Nanomaterials*, **12(21),** 3831.